Biophysical Chemistry 198 (2015) 14–21

Contents lists available at ScienceDirect

Biophysical Chemistry

journal homepage: http://www.elsevier.com/locate/biophyschem

Erythritol predicted to inhibit permeation of water and solutes through the conducting pore of *P. falciparum* aquaporin

Liao Y. Chen *

Department of Physics, University of Texas at San Antonio, One UTSA Circle, San Antonio, TX 78249, USA

HIGHLIGHTS

- Free-energy profiles of PfAQP permeants accurately computed
- Binding affinities of erythritol, glycerol, and urea computed
- Erythritol predicted to bind strongly inside PfAQP channel
- Erythritol hypothesized to inhibit *P. falciparum*

GRAPHICAL ABSTRACT

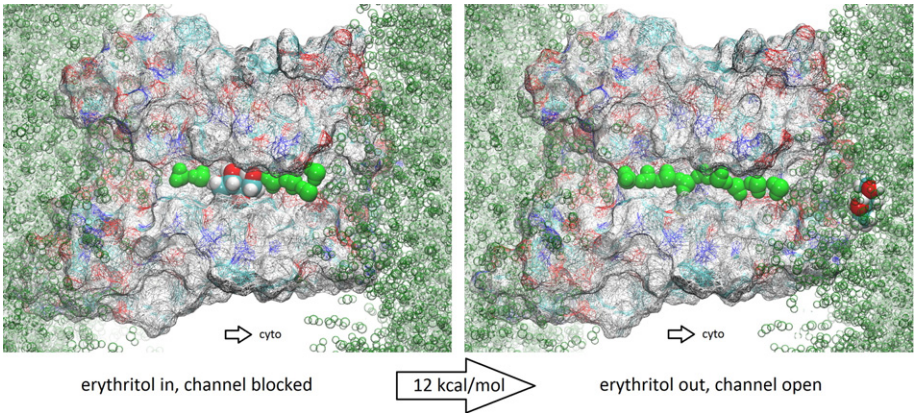

ARTICLE INFO

Article history:
Received 20 December 2014
Received in revised form 4 January 2015
Accepted 7 January 2015
Available online 14 January 2015

Keywords:
Aqua(glycero)porin
Channel-transport regulation
Polyol–protein interaction
Free energy
Malarial parasite

ABSTRACT

Plasmodium falciparum aquaporin (PfAQP) is a multifunctional channel protein in the plasma membrane of the malarial parasite that causes the most severe form of malaria infecting more than a million people a year. This channel protein facilitates transport of water and several solutes across the cell membrane. In order to better elucidate the fundamental interactions between PfAQP and its permeants and among the permeants, I conducted over three microseconds *in silico* experiments of atomistic models of the PfAQP–membrane system to obtain the free-energy profiles of five permeants (erythritol, water, glycerol, urea, and ammonia) throughout the amphipathic conducting pore of PfAQP. The profiles are analyzed in light of and shown to be consistent with the existent *in vitro* data. The binding affinities are computed using the free-energy profiles and the permeant fluctuations inside the channel. On this basis, it is predicted that erythritol, a permeant of PfAQP itself having a deep ditch in its permeation passageway, inhibits PfAQP's functions of transporting water and other solutes with an IC_{50} in the range of high nanomolars. This leads to the possibility that erythritol, a sweetener generally considered safe, may inhibit or kill the malarial parasite *in vivo* without causing undesired side effects. Experimental studies are hereby called for to directly test this theoretical prediction of erythritol strongly inhibiting PfAQP *in vitro* and possibly inhibiting *P. falciparum in vivo*.

1. Introduction

Plasmodium falciparum aquaglyceroporin (PfAQP), a member of the aquaporin family [1–7], is a multifunctional channel protein on the

* Department of Physics, One UTSA Circle, San Antonio, Texas 78249, USA. Tel.: +1 210 458 5457; fax: +1 210 458 4919.
E-mail address: Liao.Chen@utsa.edu.

http://dx.doi.org/10.1016/j.bpc.2015.01.004
0301-4622/

plasma membrane of the malarial parasite that is responsible for the most severe form of malaria infecting over a million people a year. Now we have learnt from the functional experiments that PfAQP facilitates permeation of water, glycerol, erythritol, urea, ammonia, and, possibly, ammonium across the cell membrane [8–13]. It is fundamentally and practically important to understand how these permeants interact with the protein and how they interact with one another if they coexist in the system [7,14,15]. One of the critical questions is: Could one of the permeants of PfAQP (or another aquaglyceroporin) actually inhibit the channel protein's functions of transporting other permeants? So far, *in vitro* experiments supplied us with unostentatious but unambiguous evidence that glycerol inhibits water permeation through PfAQP. The crystallization experiments aided by *in silico* simulations gave us the atomistic details of this and other aquaporin proteins, illustrating how waters and glycerols line up in a single file inside the conducting pore of this aquaglyceroporin (Fig. 1) and the *Escherichia coli* aquaglyceroporin GlpF [10,16–19]. In the absence of glycerol, *in vitro* experiments showed that water easily traverses the conducting pore of PfAQP [8] and *in silico* studies corroborated it with a flat landscape of its free energy [17,20,21]. In the presence of glycerol, *in vitro* data showed reduced water permeability of PfAQP. (This conclusion was achieved in Ref. [22] through a detailed analysis of the *in vitro* data of Refs. [10,11] in comparison with the data of Refs. [8,23,24].) And *in silico* simulations produced a free-energy profile of glycerol having a ditch [22] in its permeation path through the protein. Glycerol, when permeating through the protein channel, would dwell inside the protein for a significant time like being in a bound state and thus occlude the conducting pore of the protein. The existence of such a ditch along glycerol's permeation path is due to the structural fitness of PfAQP hosting a glycerol near the channel center where the van der Waals (vdW) interactions are all favorable between a glycerol and the lumen residues of an aquaglyceropoin.

In light of these understandings, I hypothesize that erythritol, a permeant having an even better fit than glycerol in the center of the PfAQP channel, would have a deeper ditch in its permeation path and thus would strongly inhibit PfAQP's functions of transporting water, glycerol, and other permeants (Fig. 1). This hypothesis is based on two considerations: 1. Erythritol resembles glycerol in structure (four vs

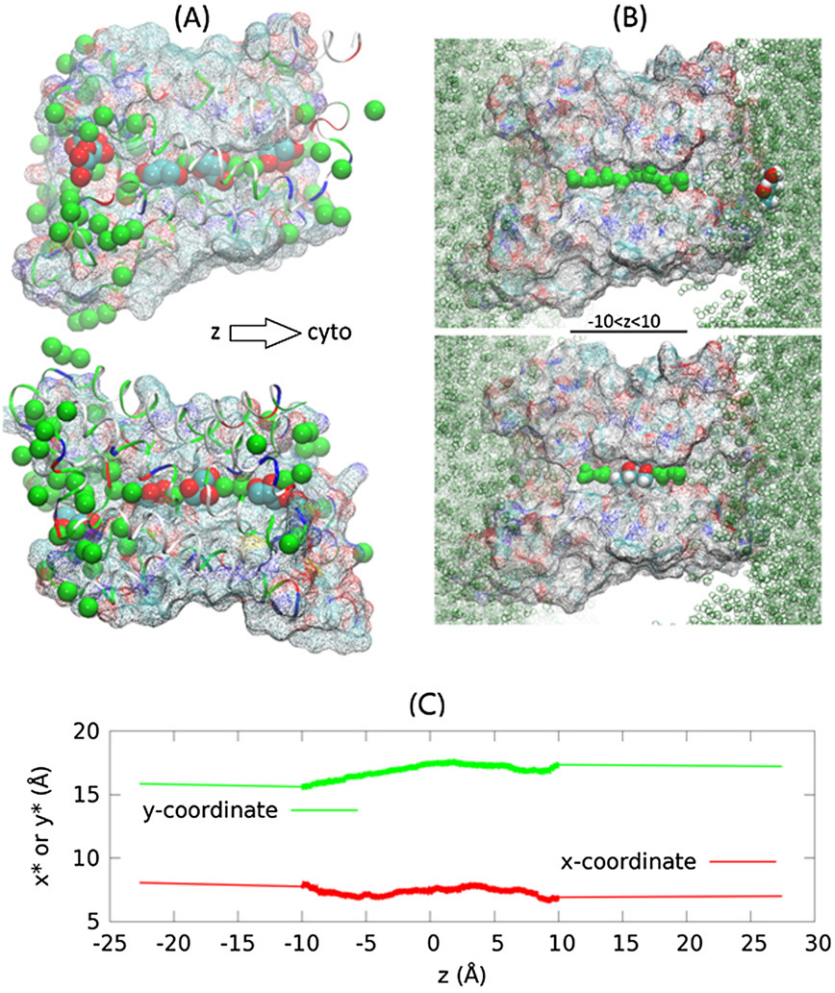

Fig. 1. (A) Shown in the left is the crystal structure of PfAQP. The coordinates are taken from the PDB (3C02) and translated along the *z*-axis so that the single-file channel region is approximately given by (-10Å $< z <$ 10Å). The protein as a whole is represented as ribbons colored by residue types. The back ($x + y >$ 22Å, top) and the front ($x + y <$ 27 Å, bottom) parts of the protein are also represented as wireframe surfaces (colored by atom names) to illustrate the conducting pore in which waters (green balls) and glycerols (red and cyan balls) line up in single file. The coordinates are so chosen that the *z*-axis points to the cytoplasmic side in perpendicular to the membrane surface. (B) Shown in the right is the equilibrated structure of PfAQP when erythritol is outside (top) and inside (bottom) the conducting pore. The single-file region of the conducting pore is indicated with the horizontal bar between the top and bottom panels. The protein is partially represented ($x + y >$ 22 Å) with wireframe surfaces colored by atom names. Erythritol is represented by white (hydrogen), cyan (carbon), and red (oxygen) balls. The waters inside the single-file channel region are represented as green balls while waters outside the single-file region are represented by green bubbles. Graphics here and in the rest of the paper were rendered with VMD [30]. (C) Shown in the bottom is the permeation path of erythritol—straight line from the extracellular bulk to the channel entry vestibule—curve inside the channel—straight line from the channel exit to the cytoplasmic bulk.

three linear carbohydroxyl groups) and thus in hydrogen bonding with waters and lumen residues lining the protein channel. 2. Erythritol is bulkier than glycerol but the PfAQP channel has sufficient room near the Asn-Leu-Ala (NLA) and Asn-Pro-Ser (NPS) motifs to accommodate the molecule having all favorable vdW interactions with the lumen residues. (The room there is more than enough for a glycerol and therefore glycerol binding there is not the maximum fit.) These two factors combined would give rise to stronger binding of erythritol near the NLA-NPS motifs. To theoretically validate this hypothesis, we need an accurate determination of the free-energy profile for each permeant—the potential of mean force (PMF) [25–29] as a function of the permeant center-of-mass (COM) coordinates along its permeation path leading from the periplasm to the entry vestibule of PfAQP, throughout the channel, to the cytoplasm (see Fig. 1(C) for an illustration of the permeation path of erythritol. Note that the coordinates are chosen as follows: The xy-plane is located near the center of the PfAQP channel and parallel to the membrane-cyto/periplasm interfaces and the *z*-axis points from the periplasmic to the cytoplasmic side.) These free-energy profiles along with the permeant fluctuations inside the channel, considered on the basis of the structure information available in the literature, can ascertain the conclusion that erythritol inhibits PfAQP in the concentration range of high nanomolars.

In this paper, I present the free-energy profiles for the five permeants (erythritol, water, glycerol, urea, and ammonia) computed on the basis of circa 3 μs molecular dynamics (MD) simulations, which amount to more than ten times the computational efforts invested on an aquaglyceroporin in the current literature. The free-energy profile of each of the permeants is computed as the PMF along the most probable path from the extracellular bulk, through the PfAQP channel, to the cytoplasmic bulk. Erythritol is found to have the strongest binding with PfAQP. It's free-energy curve has a very deep well inside the PfAQP channel near the NLA-NPS motifs that is 12 kcal/mol below its free energy in the bulk of periplasm/cytoplasm. Using this profile along with the erythritol fluctuations inside the channel, the dissociation constant is computed to be 786 nM. When an erythritol molecule is dissociated from and bound to the ditch inside the protein's conducting pore, PfAQP will switch between being open and closed to permeation of water or other permeants (Fig. 1). Therefore, one can readily regulate PfAQP's functions of transporting water and other permeants by adjusting the erythritol concentration in the nM to μM range. Even though direct validation of this theory of erythritol inhibiting PfAQP needs further *in vitro* experiments measuring the erythritol-PfAQP dissociation constant and the protein's permeabilities for various erythritol concentrations, the *in vitro* data available in the current literature do support various biophysical implications of the results of this work.

2. Methods

2.1. System setup

This study was based on the following all-atom model of PfAQP embedded in the cell membrane (illustrated in supplemental Fig. S1), similar to Refs. [31,32]. The PfAQP–membrane system with glycerols was fully described in Ref. [22]. Briefly, the PfAQP tetramer including the structural waters, formed from the crystal structure (PDB code: 3C02), was embedded in a patch of fully hydrated palmitoyloleylphosphatidyl–ethanolamine (POPE) bilayer. The PfAQP–POPE complex is sandwiched by two layers of water, each of which is approximately 30 Å in thickness. The system is neutralized with 9 Cl^- ions. And additional Na^+ and Cl^- ions were added at a concentration of 150 mM. The entire system, consisting of 150,459 atoms, is 116 Å × 114 Å × 107 Å in dimension when fully equilibrated. The Cartesian coordinates are chosen such that the origin is at the geometric center of the PfAQP tetramer. The xy-plane is parallel to the lipid–water interface and the *z*-axis is pointing from the periplasm to the cytoplasm. The PfAQP–membrane systems with ammonia, urea, and erythritol were, respectively, built by replacing glycerols with the corresponding permeants. For the study of water permeation, the PfAQP–membrane system was obtained by deleting all the glycerols.

All the simulations of this work were performed using NAMD 2.9 [33]. The all-atom CHARMM36 parameters [34–36] were adopted for inter- and intra-molecular interactions without modifications except for urea in which case the parameters of Ref. [37] were used instead. Water was represented explicitly with the TIP3 model. The pressure and the temperature were maintained at 1 bar and 293.15 K, respectively. The Langevin damping coefficient was chosen to be 5/ps. The periodic boundary conditions were applied to all three dimensions, and the particle mesh Ewald was used for the long-range electrostatic interactions. Covalent bonds of hydrogens were fixed to their equilibrium length. The time step of 1 fs was used for short-range interactions and 4 fs was used for long-range forces. The cut-off for long-range interactions was set to 12 Å with a switching distance of 10 Å. In all simulations, the alpha carbons on the trans-membrane helices of PfAQP within the range of $-10\text{Å} < z < 10$ Å were fixed to fully respect the crystal structure.

2.2. Steered molecular dynamics (SMD)

SMD [38–40] runs were conducted to sample the transition paths of each of the permeating molecules (erythritol, water, glycerol, urea, ammonia) going from the periplasm, through the conducting pore, to the cytoplasm, for computing the free-energy profiles. The entire permeation path leading from the periplasm ($z < -20$ Å), through the PfAQP pore, to the cytoplasm bulk region ($z > 20$ Å), was divided into multiple sections of 1.0 Å each in width. In each section, a chosen permeant's COM was steered/pulled in the positive *z*-direction to sample a forward pulling path, and then pulled in the negative *z*-direction to sample a reverse pulling path. The pulling speed was $v = 2.5$ Å/ns in both directions. Four forward paths and four reverse paths were sampled in every section. 4.0 ns equilibration was performed at both end points of each section so that the pulling paths were sampled between equilibrium states with the permeant's COM coordinates being fixed at the desired values. In the single-file region inside the conducting pore ($z_1 < z < z_2$), the *z*-coordinate of the pulled molecule's COM was advanced with the constant velocity given above while the *x*- and *y*-degrees of freedom were left uncontrolled to obey the system's dynamics. Thus the *x*- and *y*-coordinates fluctuate around the free energy minimum $(x^*(z), y^*(z))$ on the *xy*-plane at a given *z*-coordinate. The COM of the pulled molecule approximately follows the most probable path $(x^*(z), y^*(z), z)$ as it is pulled in the *z*-direction. In the non-single-file regions from the channel entry vestibule to the extracellular bulk and from the channel exit to the cytoplasmic bulk, the *z*-coordinate was advanced in the same manner as in the single-file region but the *x*- and *y*-degrees of freedom were fixed to their constant values $(x^*(z_1), y^*(z_1))$ on the extracellular side and $(x^*(z_2), y^*(z_2))$ on the cytoplasmic side respectively. The formulae of Ref. [41] were used for extracting the free-energy profiles from the simulation data and for computing the dissociation constants. They are restated below.

The 1D PMF in the single-file region, $G_{1D}(z)$, can be computed through the Brownian dynamics fluctuation–dissipation theorem (BD-FDT) [42] as follows:

$$G_{1D}(z) - G_{1D}(z_A) = -k_B T \ln\left(\frac{\langle \exp[-W_{A\to Z}/2k_BT]\rangle_F}{\langle \exp[-W_{Z\to A}/2k_BT]\rangle_R}\right). \quad (1)$$

Here the COM *z*-coordinate of the permeant is pulled while the *x*- and *y*-coordinates are free to fluctuate. Along each forward pulling path from A to B, the work done to system was recorded as $W_{A\to Z}$ when the permeant was pulled from A to Z. Along each reverse pulling path from B to A, the work done to system was recorded as $W_{B\to Z}$ when the permeant was pulled from B to Z. Here Z represents a state of the

system when the COM z-coordinate of the pulled permeant is z. A and B represent two end states of a given section, respectively. $W_{Z\to A} = W_{B\to A} - W_{B\to Z}$ is the work done to the system for the part of a reverse path when the permeant was pulled from Z to A. k_B is the Boltzmann constant and T is the absolute temperature. z_A and z_B are the z-coordinates of the COM of the pulled permeant at the end states A and B of the system, respectively.

The 3D PMF in the non-single-file regions outside the channel, $G_{3D}(x, y, z)$, as a function of the permeant COM position (x,y,z), can also be computed with the BD-FDT:

$$G_{3D}(x,y,z) - G_{3D}(x_A,y_A,z_A) = -k_BT \ln\left(\frac{\langle \exp[-W_{A\to Z}/2k_BT]\rangle_F}{\langle \exp[-W_{Z\to A}/2k_BT]\rangle_R}\right) \quad (2)$$

when the pulling is conducted along a straight line or a fixed curve. Note that only the z-components of the pulling forces were necessary for computing the work done to the pulled molecule in both the single-file and the non-single-file regions because the x- and y-coordinates were either not pulled or not allowed any displacements. In both cases, only the z-components contribute to the work done.

The 3D PMF along the most probable path inside the single-file channel region is related to the 1D PMF,

$$G_{3D}(x*(z), y*(z), z) = G_{1D}(z) + k_BT \ln(A(z)/A(z_1)) \quad (3)$$

where the area ratio can be approximated by computing the determinant of the variance matrix of the COM x- and y-coordinates of the permeant,

$$A(z)/A(z_1) = \left(\begin{vmatrix} \langle \delta x^2 \rangle_z & \langle \delta x \delta y \rangle_z \\ \langle \delta x \delta y \rangle_z & \langle \delta y^2 \rangle_z \end{vmatrix} \Big/ \begin{vmatrix} \langle \delta x^2 \rangle_{z_1} & \langle \delta x \delta y \rangle_{z_1} \\ \langle \delta x \delta y \rangle_{z_1} & \langle \delta y^2 \rangle_{z_1} \end{vmatrix} \right)^{1/2}. \quad (4)$$

Here $\delta x = x - x^*(z)$ and $\delta y = y - y^*(z)$ denote deviations from the most probable path. The brackets with subscript z mean the statistical average on the xy-plane of a given z coordinate. The area $A(z_1)$ is taken as the reference area.

2.3. Computing the dissociation constant

Following Ref. [29], we have the binding constant

$$\begin{aligned} c_0/k_d &= c_0 \iiint_{\substack{\text{single-file}\\ \text{region}}} dxdydz \exp[-G_{3D}[x,y,z]/k_BT] \\ &= c_0 A(z_1) \int_{z_1}^{z_2} dz \exp[-G_{1D}[z]/k_BT]. \end{aligned} \quad (5)$$

In Eq. (5), we use, for convenience of unit conversions, two different but equivalent forms of the standard concentration, $c_0 = 1M$ on the left hand side and $c_0 = 6.02\times10^{-4}\text{Å}^{-3}$ on the right hand side. k_d is the dissociation constant. The PMF in the bulk is chosen to be zero.

3. Results and discussion

Shown in Fig. 2 are free-energy profiles (from top panel down) for water, ammonia, urea, glycerol, and erythritol, respectively, each of which is the PMF (kcal/mol) as a function of the permeant's COM z-coordinate (Å) along a permeation path across the cell membrane through the conducting pore of PfAQP. Note that the single file channel region is between $z_1 = -10\text{Å}$ and $z_2 = 10\text{Å}$ as shown in Fig. 1. Each PMF curve represents the free-energy variation as a function of a permeant's COM z-coordinate along a permeation path consisting of a line $(x^*(z_1), y^*(z_1), z)$ leading from the periplasmic bulk $(z < -20\text{Å})$ to the channel entry $(z = z_1)$, a curve $(x^*(z), y^*(z), z)$—the most probable path inside the conducting pore,

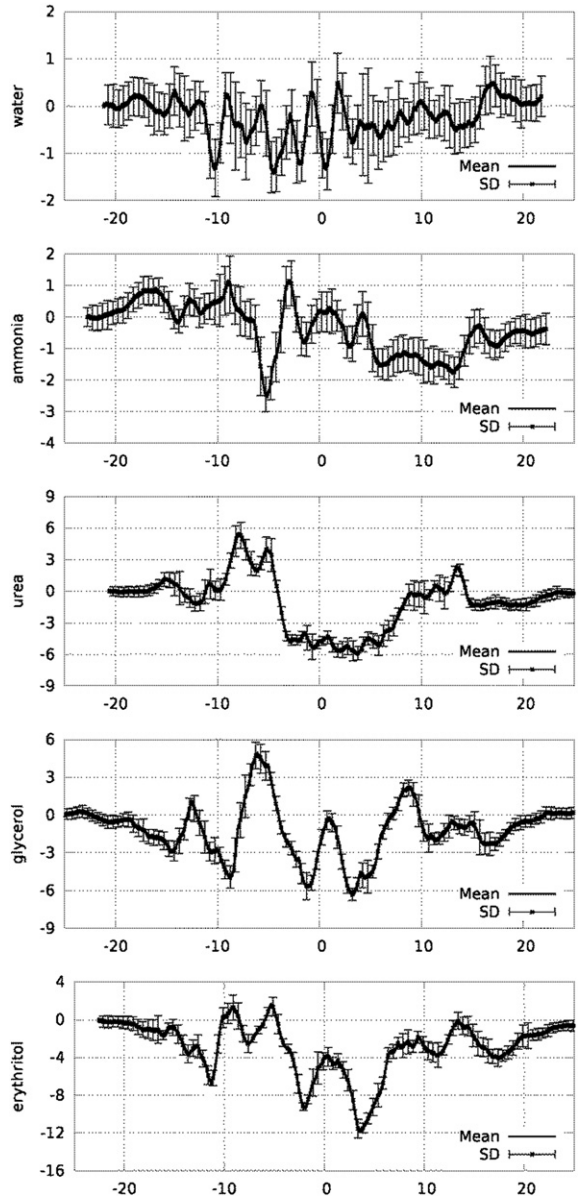

Fig. 2. Free-energy profiles of water and solutes along the permeation passageway through the conducting pore of PfAQP:PMF (kcal/mol) as a function of the z-coordinate (Å) of the permeating molecule. On the periplasmic side, the profiles represent the PMF along the straight line: $(x_1{}^*, y_1{}^*, z)$ leading from the extracellular bulk $(z < -20\text{Å})$ to the channel entry $(x_1{}^*, y_1{}^*, z_1 = -10\text{Å})$. Inside the single-file channel region $(z_1 < z < z_2)$, the profiles represent the PMF along the most probable path $(x^*(z), y^*(z), z)$. On the cytoplasmic side, the profiles represent that the PMF is along the straight line $(x_2{}^*, y_2{}^*, z)$ leading from the channel exit $(x_2{}^*, y_2{}^*, z_2 = 10\text{Å})$ to the cytoplasmic bulk $(z > 20\text{Å})$. Here $(x_1^* = x^*(z_1), y_1^* = y^*(z_1))$ and $(x_2^* = x^*(z_2), y_2^* = y^*(z_2))$ are, respectively, the xy-coordinates of the most probable path at the channel entry and at the channel exit.

and another line $(x^*(z_2), y^*(z_2), z)$ leading from the channel exit $(z = z_2)$ to the cytoplasmic bulk $(z > 20\text{Å})$. The entire permeation path of erythritol is illustrated in Fig. 1(C). For all of the five neutral permeants, the chemical potential in the extracellular bulk is, within the margin of error, equal to that in the cytoplasmic bulk, indicating validity of the computation. These five free-energy curves are difficult to confirm experimentally but their biophysical implications can be readily validated. They are in fact consistent with the existent *in vitro* data available in the current literature. Further validation can be achieved with

more experiments measuring the binding affinities and the permeation regulations.

3.1. Water permeation through PfAQP vs AQPZ

The top panel of Fig. 2 shows the PMF for water permeation that has multiple shallow minima and low maxima. The difference between the highest maximum and the deepest minimum within the single-file region gives the Arrhenius activation barrier for water permeation that is approximately 2.0 kcal/mol. This profile means high water permeability of PfAQP in full agreement with the *in vitro* findings [8,10] that PfAQP is as efficient as the water specific aquaporins AQP1, AQP4, and AQPZ. Inhibiting this highly efficient function in water permeation would seriously reduce the parasite's ability of maintaining hydro-homeostasis across its plasma membrane when it is subject to severe osmotic stress during renal circulations. Inside the PfAQP channel, there are seven minima whose locations correspond well with the locations of waters shown in Fig. 1 (top right illustration). This feature of PfAQP is similar to AQPZ whose crystal structure [43] demonstrates the single-file line of waters inside the conducting pore illustrated in Fig. 3. Quantitatively, I computed the free-energy profile of water permeating through AQPZ (Fig. 3) in the same way as for PfAQP, predicting an Arrhenius activation barrier of 3.4 ± 0.6 kcal/mol for water transport that is in agreement with the experimental value of 3 kcal/mol [23] and consistent with recent *in silico* studies of AQP4 [31,32]. The agreement between this *in silico* prediction and the *in vitro* studies of AQPZ should strongly indicate the validity of the approach of this work.

3.2. Ammonia

The second panel of Fig. 2 shows that the PMF curve for ammonia permeation is rather shallow as well. Its deepest well is −2.5 kcal/mol and its highest barrier is only 1.1 kcal/mol. The Arrhenius activation barrier of ammonia permeation is approximately 3.6 kcal/mol. Therefore, PfAQP facilitates ammonia transport across the plasma membrane of *P. falciparum* at a very high efficiency, in agreement with the *in vitro* findings of Ref. [12]. Inhibiting this function of PfAQP may severely harm the parasite's metabolism if *P. falciparum* indeed relies on PfAQP for excretion of this metabolic waste.

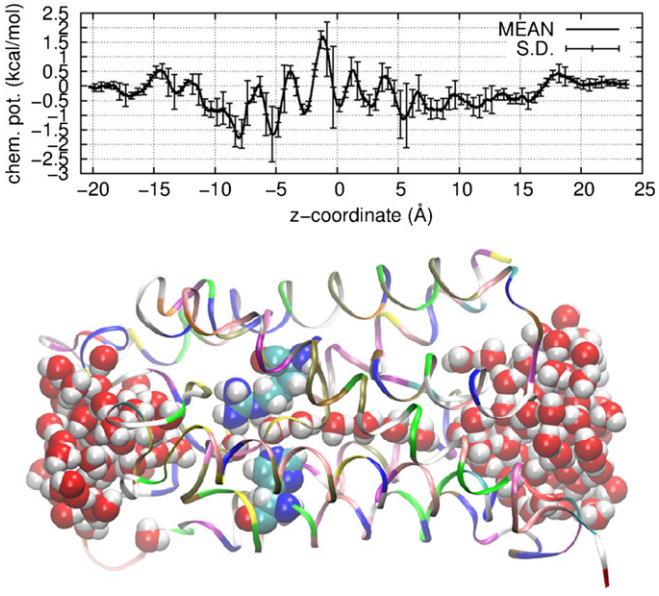

Fig. 3. Water permeation through AQPZ. Shown in the top panel is the free-energy profile, the PMF as a function of the COM *z*-coordinate of a water molecule. Shown in the bottom panel is the protein in ribbons colored by residue name along with waters in red (oxygen) and white (hydrogen) spheres within the conducting pore of AQPZ and near the channel entry and exit. Also shown are residues at the narrowest part of the channel, ARG 189 and HIS 174 in spheres colored by atom names.

3.3. Glycerol vs urea

The third and fourth panels of Fig. 2 show that the free-energy profiles of urea and glycerol both have deep ditches inside the single-file channel regions. Urea and glycerol, when permeating PfAQP, are both subject to the process of being bound inside the protein (dwelling inside the channel for significant times), occluding the channel from conducting water or ammonia. The binding affinities of urea and glycerol are similar, both in the low mM range. In terms of dissociation constant, we have $k_d^{urea} = 1.3$ mM and $k_d^{gol} = 1.8$ mM, using Eq. (5) that involves fluctuations of urea and glycerol shown in supplemental figures S2 to S4. Note that the dissociation constant of urea is significantly smaller than that of glycerol because the urea has greater entropy than glycerol at the binding site inside the conducting pore. Glycerol is about 50% bulkier than urea and thus has less space to fluctuate inside the pore. Its binding to PfAQP is weaker than urea even though the ditch in its PMF curve (−6.5 kcal/mol) is slightly deeper than urea (−6.0 kcal/mol). The difference between urea and glycerol is within the margin of error. Also note that Ref. [22] did not take full account of this entropic contribution to give an accurate estimate of the glycerol–PfAQP dissociation constant. The PMF value of −6.5 kcal/mol was regarded in Ref. [22] as the sole contribution to the binding free-energy. Taking full account of all contributions to the binding free energy, one needs to use Eq. (5) as it is done this work.

Based on the binding constants and the fact that PfAQP only allows single-file of waters and solutes inside the conducting pore, it is predicted that, in the mM concentration range, either urea or glycerol inhibits water/ammonia permeation through PfAQP. In the presence of high concentration of glycerol/urea, PfAQP will be saturated with glycerol/urea inside its channel. Then water permeation is fully correlated to the off rate of glycerol/urea and thus will have an activation barrier (over 6 kcal/mol) that is significantly higher than the barrier (around 2 kcal/mol) in the absence of glycerol/urea. The current literature does not have all the data to fully validate this theoretical prediction but a careful analysis of the existent *in vitro* experiments was done in Ref. [41] showing that the presence of glycerol suppresses water conduction through aquaglyceroporin. For example, "Song *et al.* [11] examined water permeability of PfAQP expressed in protoplasts. They determined the rate constants from the exponential fitting of their light scattering curves. The rate constants so determined are proportional to the water permeation rates across the protoplasts. They extracted the difference between the rate of PfAQP-expressing protoplasts and the rate of the non-expressing control protoplasts for different osmolytes including glycerol. For 300 mosM across the protoplasts induced by sucrose in the absence of glycerol, the rate difference was 0.3/s. For the same 300 mosM induced by glycerol, the rate difference was only 0.01/s, indicating that the PfAQP was completely inhibited at high glycerol concentration."

Another similarity between glycerol and urea is that the highest barriers of their free-energy profiles are both in the ar/r selectivity-filter region ($z \sim -7$Å). And the deepest wells are located near the NPS-NLA motifs ($z \sim 4$Å) where the channel is widest to accommodate the solutes without significant distortion in the channel-lining side-chains of the protein. The Arrhenius activation barriers (equal to the difference between the highest peak and the lowest trough) are both approximately 11 kcal/mol. Currently, *in vitro* experiments are needed to measure the activation barriers and to measure the dissociation constants of urea and glycerol. Note, however, that the Arrhenius activation barrier for glycerol permeation through GlpF was measured to be 9.7 kcal/mol [23]. This experimentally measured value validates GlpF's free-energy profile computed in Ref. [41] that resembles PfAQP's profile discussed above.

3.4. Erythritol

The fifth panel of Fig. 2 shows the free-energy profile of erythritol permeation. The activation barrier of erythritol permeation is higher than that of glycerol. Therefore, PfAQP is less permeable to erythritol than to glycerol. This conclusion is in agreement with the *in vitro* data of Ref. [8]. There is a very deep ditch (about 12 kcal/mol below the bulk level) in erythritol's permeation path inside the PfAQP channel near the NLA-NPS motifs. This means that erythritol is tightly bound to PfAQP inside the conducting pore. The dissociation constant of erythritol from the PfAQP pore is estimated to be $k_d^{ery} = 786$ nM, using Eq. (5) that utilizes erythritol fluctuations inside the conducting pore illustrated in supplemental figures S5 and S6. The binding affinity of erythritol is much stronger than urea or glycerol. Therefore, the presence of glycerol or urea in the system will not inhibit the permeation of erythritol through the PfAQP pore, in agreement with the *in vitro* data [8]. Conversely, the presence of erythritol will inhibit the transport of glycerol and urea. The current literature does not have experimental data to support or to contradict this latter biophysical implication of the free-energy profiles that erythritol strongly modulates the function of PfAQP in facilitating transport of water and solutes across the cell membrane. *In vitro* experiments are needed to measure the PfAQP–erythritol dissociation constant and to measure the PfAQP permeabilities of water, ammonia, glycerol, and urea in the presence of erythritol at various concentrations from high nM to μM.

Finally, what atomistic interactions are responsible for the free-energy profile of erythritol permeation having a deep ditch near the NLA-NPS motifs? This question can be answered with Fig. 4 about the van der Waals interactions between erythritol and the lumen residues of PfAQP along with some other structural and energetic insights. In particular, there is a very deep well (−18kcal/mol) in the curve of the van der Waals interaction energy between erythritol and PfAQP as a function of the *z*-coordinate of the erythritol COM along the permeation path, demonstrating very strong attraction between the protein and erythritol inside the channel near the NPS-NLA motifs. This strong attraction is due to the fact that the structure of this aquaglyceroporin has a "perfect" binding site for erythritol near the NPS-NLA motifs. It can host an erythritol there fitly (Fig. 4(B)) without any repulsive contact between the lumen residues and erythritol (Fig. 4(B), (D), (F) in contrast with (A), (E)). The van der Waals interactions between

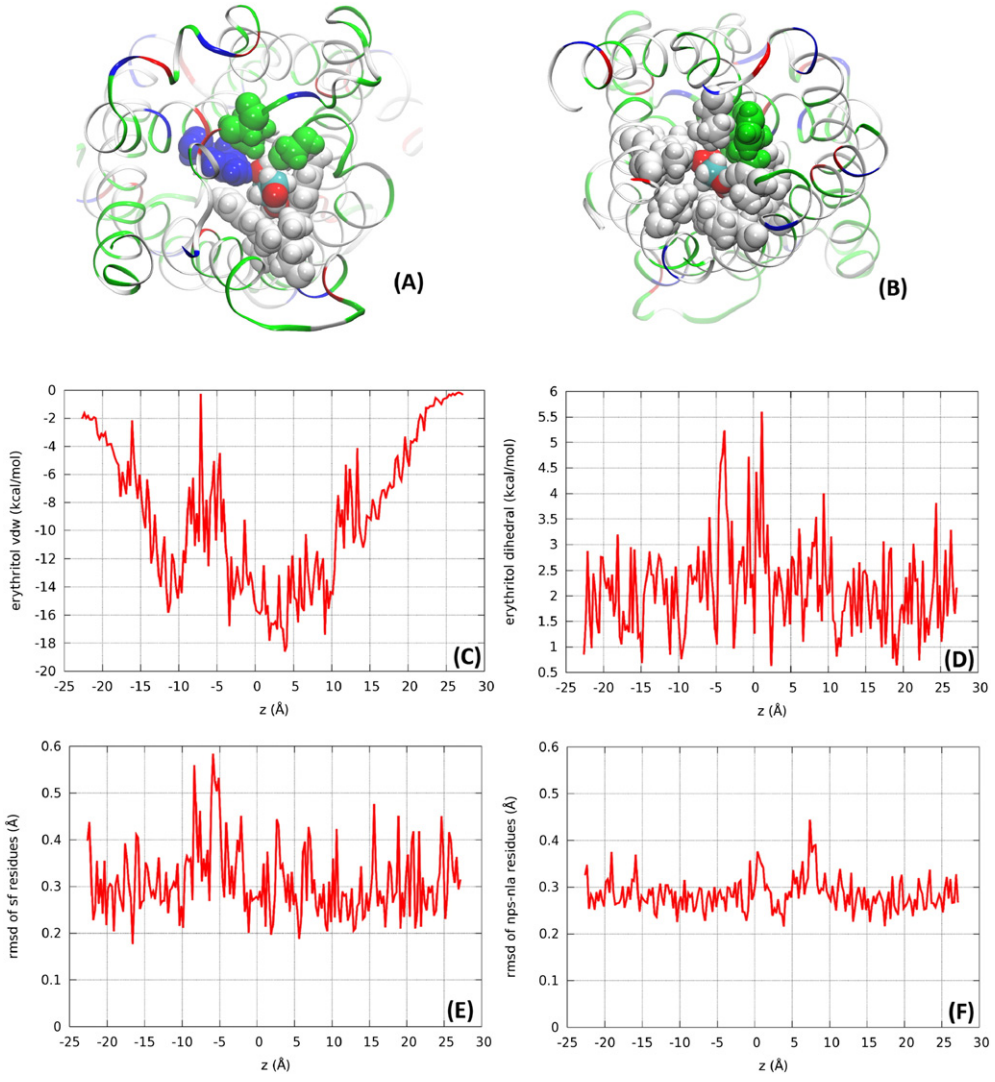

Fig. 4. (A) PfAQP in ribbons colored by residue types with erythritol in red (oxygen), white (hydrogen), and cyan (carbon) balls. The COM of erythritol is located $z = -6$ Å. Also shown in balls colored by residue types are six residues in repulsive contact with (distance < 2.3 Å from) erythritol: L46, W50, T126, G189, P190, and R196. Viewed from periplasmic side. (B) The protein and erythritol are represented in the same way as in (A) but viewed from the cytoplasmic side. The COM of erythritol is located at $z = 4$ Å, near the NPS-NLA motifs. Also shown are the 12 residues in balls colored by residue types that are in favorable contact with (distance 2 to 3 Å from) erythritol: L23, V54, I58, A67, H68, L69, N70, V73, L148, I152, V173, and N193. (C) The van der Waals interaction energy between erythritol and the protein as a function of the erythritol COM coordinate. (D) The dihedral energy of erythritol. (E) The RMSD of the six residues listed in (A). (F) The RMSD of the 12 residues listed in (B).

erythritol and PfAQP are all favorable over there. These favorable interactions are responsible for the free-energy profile of erythritol (Fig. 2, bottom panel) because the number of hydrogen bonds formed by erythritol with the lumen residues and the waters inside the channel do not vary drastically throughout the channel.

4. Conclusions

The multi-functional channel protein PfAQP is capable of facilitating transport of water, ammonia, urea, glycerol, and erythritol across the *P. falciparum* plasma membrane. Water and ammonia can traverse the protein's conducting pore without dwelling inside the channel much longer than occupying another space of similar volume in the bulk because their free-energy profiles do not have deep ditches along their permeation paths through the channel. In contrast, urea, glycerol, and erythritol all have deep ditches along their permeation paths. They all dwell inside the channel with a much greater probability than occupying a similar space in the bulk regions. Therefore, the presence of any of these three solutes in the system modulates the permeation of water and ammonia. Glycerol's ditch has a depth (−6.5 kcal/mol) similar to urea's (−6.0 kcal/mol) and, therefore, the two mutually interfere with one another's transport. Finally and most importantly, the ditch along erythritol's permeation path (−12 kcal/mol) is much deeper than those of urea and glycerol. The presence of erythritol strongly regulates PfAQP's multifunctional capabilities. These conclusions can be considered partially validated because they do not contradict any but agree with all the *in vitro* data that are available in the current literature. They are still to be fully validated with more *in vitro* studies to measure transport regulations with a range of urea, glycerol, and erythritol concentrations and to measure the dissociation constants for urea, glycerol, and erythritol.

Declaration of interest

The author declares no conflict of interest.

Acknowledgments

The author thanks Dr. Q. Zhou for helpful discussions. He acknowledges support from the NIH (#GM084834) and the Texas Advanced Computing Center.

Appendix A. Supplementary data

Supplementary data to this article can be found online at http://dx.doi.org/10.1016/j.bpc.2015.01.004.

References

[1] P. Agre, M. Bonhivers, M.J. Borgnia, The aquaporins, blueprints for cellular plumbing systems, J. Biol. Chem. 273 (1998) 14659–14662.
[2] A. Engel, H. Stahlberg, Aquaglyceroporins: channel proteins with a conserved core, multiple functions, and variable surfaces, in: W.D.S. Thomas Zeuthen (Ed.), International Review of Cytology, Academic Press, 2002, pp. 75–104.
[3] J.M. Carbrey, P. Agre, Discovery of the Aquaporins and Development of the Field Aquaporins, in: E. Beitz (Ed.), Springer, Berlin Heidelberg, 2009, pp. 3–28.
[4] K. Hedfalk, N. Pettersson, F. Oberg, S. Hohmann, E. Gordon, Production, characterization and crystallization of the *Plasmodium falciparum* aquaporin, Protein Expr. Purif. 59 (2008) 69–78.
[5] J.K. Lee, S. Khademi, W. Harries, D. Savage, L. Miercke, R.M. Stroud, Water and glycerol permeation through the glycerol channel GlpF and the aquaporin family, J. Synchrotron Radiat. 11 (2004) 86–88.
[6] G. Benga, On the definition, nomenclature and classification of water channel proteins (aquaporins and relatives), Mol. Asp. Med. 33 (2012) 514–517.
[7] A.S. Verkman, M.O. Anderson, M.C. Papadopoulos, Aquaporins: important but elusive drug targets, Nat. Rev. Drug Discov. 13 (2014) 259–277.
[8] M. Hansen, J.F. Kun, J.E. Schultz, E. Beitz, A single, bi-functional aquaglyceroporin in blood-stage *Plasmodium falciparum* malaria parasites, J. Biol. Chem. 277 (2002) 4874–4882.
[9] E. Beitz, S. Pavlovic-Djuranovic, M. Yasui, P. Agre, J.E. Schultz, Molecular dissection of water and glycerol permeability of the aquaglyceroporin from *Plasmodium falciparum* by mutational analysis, Proc. Natl. Acad. Sci. U. S. A. 101 (2004) 1153–1158.
[10] Z.E. Newby, J. O'Connell III, Y. Robles-Colmenares, S. Khademi, L.J. Miercke, R.M. Stroud, Crystal structure of the aquaglyceroporin PfAQP from the malarial parasite *Plasmodium falciparum*, Nat. Struct. Mol. Biol. 15 (2008) 619–625.
[11] J. Song, A. Almasalmeh, D. Krenc, E. Beitz, Molar concentrations of sorbitol and polyethylene glycol inhibit the Plasmodium aquaglyceroporin but not that of *E. coli*: involvement of the channel vestibules, Biochim. Biophys. Acta Biomembr. 1818 (2012) 1218–1224.
[12] T. Zeuthen, B. Wu, S. Pavlovic-Djuranovic, L.M. Holm, N.L. Uzcategui, M. Duszenko, J.F. Kun, J.E. Schultz, E. Beitz, Ammonia permeability of the aquaglyceroporins from *Plasmodium falciparum*, *Toxoplasma gondii* and *Trypansoma brucei*, Mol. Microbiol. 61 (2006) 1598–1608.
[13] L. Holm, T. Jahn, A.B. Møller, J. Schjoerring, D. Ferri, D. Klaerke, T. Zeuthen, NH3 and NH4+ permeability in aquaporin-expressing Xenopus oocytes, Pflugers Arch. 450 (2005) 415–428.
[14] J. Song, E. Mak, B. Wu, E. Beitz, Parasite aquaporins: current developments in drug facilitation and resistance, Biochim. Biophys. Acta Gen. Subj. 1840 (2014) 1566–1573.
[15] S. Pavlovic-Djuranovic, J.F.J. Kun, J.E. Schultz, E. Beitz, Dihydroxyacetone and methylglyoxal as permeants of the Plasmodium aquaglyceroporin inhibit parasite proliferation, Biochim. Biophys. Acta Biomembr. 1758 (2006) 1012–1017.
[16] D. Fu, A. Libson, L.J.W. Miercke, C. Weitzman, P. Nollert, J. Krucinski, R.M. Stroud, Structure of a glycerol-conducting channel and the basis for its selectivity, Science 290 (2000) 481–486.
[17] B.L. de Groot, H. Grubmüller, Water permeation across biological membranes: mechanism and dynamics of aquaporin-1 and GlpF, Science 294 (2001) 2353–2357.
[18] E. Tajkhorshid, P. Nollert, M.Ø. Jensen, L.J.W. Miercke, J. O'Connell, R.M. Stroud, K. Schulten, Control of the selectivity of the aquaporin water channel family by global orientational tuning, Science 296 (2002) 525–530.
[19] F. Zhu, E. Tajkhorshid, K. Schulten, Theory and simulation of water permeation in aquaporin-1, Biophys. J. 86 (2004) 50–57.
[20] C. Aponte-Santamaria, J.S. Hub, B.L. de Groot, Dynamics and energetics of solute permeation through the *Plasmodium falciparum* aquaglyceroporin, Phys. Chem. Chem. Phys. 12 (2010) 10246–10254.
[21] J.S. Hub, B.L. de Groot, Mechanism of selectivity in aquaporins and aquaglyceroporins, Proc. Natl. Acad. Sci. U. S. A. 105 (2008) 1198–1203.
[22] L.Y. Chen, Glycerol inhibits water permeation through *Plasmodium falciparum* aquaglyceroporin, J. Struct. Biol. 181 (2013) 71–76.
[23] M.J. Borgnia, P. Agre, Reconstitution and functional comparison of purified GlpF and AqpZ, the glycerol and water channels from *Escherichia coli*, Proc. Natl. Acad. Sci. U. S. A. 98 (2001) 2888–2893.
[24] M.L. Zeidel, S.V. Ambudkar, B.L. Smith, P. Agre, Reconstitution of functional water channels in liposomes containing purified red cell CHIP28 protein, Biochemistry 31 (1992) 7436–7440.
[25] J.G. Kirkwood, Statistical mechanics of fluid mixtures, J. Chem. Phys. 3 (1935) 300–313.
[26] D. Chandler, Statistical mechanics of isomerization dynamics in liquids and the transition state approximation, J. Chem. Phys. 68 (1978) 2959–2970.
[27] M.K. Gilson, J.A. Given, B.L. Bush, J.A. McCammon, The statistical-thermodynamic basis for computation of binding affinities: a critical review, Biophys. J. 72 (1997) 1047–1069.
[28] B. Roux, Statistical mechanical equilibrium theory of selective ion channels, Biophys. J. 77 (1999) 139–153.
[29] T.W. Allen, O.S. Andersen, B. Roux, Molecular dynamics — potential of mean force calculations as a tool for understanding ion permeation and selectivity in narrow channels, Biophys. Chem. 124 (2006) 251–267.
[30] W. Humphrey, A. Dalke, K. Schulten, VMD: visual molecular dynamics, J. Mol. Graph. 14 (1996) 33–38.
[31] D. Alberga, O. Nicolotti, G. Lattanzi, G.P. Nicchia, A. Frigeri, F. Pisani, V. Benfenati, G.F. Mangiatordi, A new gating site in human aquaporin-4: insights from molecular dynamics simulations, Biochim. Biophys. Acta Biomembr. 1838 (2014) 3052–3060.
[32] Y. Cui, D.A. Bastien, Water transport in human aquaporin-4: molecular dynamics (MD) simulations, Biochem. Biophys. Res. Commun. 412 (2011) 654–659.
[33] J.C. Phillips, R. Braun, W. Wang, J. Gumbart, E. Tajkhorshid, E. Villa, C. Chipot, R.D. Skeel, L. Kalé, K. Schulten, Scalable molecular dynamics with NAMD, J. Comput. Chem. 26 (2005) 1781–1802.
[34] A.D. MacKerell, N. Banavali, N. Foloppe, Development and current status of the CHARMM force field for nucleic acids, Biopolymers 56 (2000) 257–265.
[35] B.R. Brooks, C.L. Brooks, A.D. Mackerell, L. Nilsson, R.J. Petrella, B. Roux, Y. Won, G. Archontis, C. Bartels, S. Boresch, A. Caflisch, L. Caves, Q. Cui, A.R. Dinner, M. Feig, S. Fischer, J. Gao, M. Hodoscek, W. Im, K. Kuczera, T. Lazaridis, J. Ma, V. Ovchinnikov, E. Paci, R.W. Pastor, C.B. Post, J.Z. Pu, M. Schaefer, B. Tidor, R.M. Venable, H.L. Woodcock, X. Wu, W. Yang, D.M. York, M. Karplus, CHARMM: the biomolecular simulation program, J. Comput. Chem. 30 (2009) 1545–1614.
[36] K. Vanommeslaeghe, E. Hatcher, C. Acharya, S. Kundu, S. Zhong, J. Shim, E. Darian, O. Guvench, P. Lopes, I. Vorobyov, A.D. Mackerell, CHARMM general force field: a force field for drug-like molecules compatible with the CHARMM all-atom additive biological force fields, J. Comput. Chem. 31 (2010) 671–690.
[37] L.J. Smith, H.J.C. Berendsen, W.F. van Gunsteren, Computer simulation of urea–water mixtures: a test of force field parameters for use in biomolecular simulation, J. Phys. Chem. B 108 (2003) 1065–1071.
[38] B. Isralewitz, J. Baudry, J. Gullingsrud, D. Kosztin, K. Schulten, Steered molecular dynamics investigations of protein function, J. Mol. Graph. Model. 19 (2001) 13–25.
[39] S. Park, K. Schulten, Calculating potentials of mean force from steered molecular dynamics simulations, J. Chem. Phys. 120 (2004) 5946–5961.

[40] L.Y. Chen, Exploring the free-energy landscapes of biological systems with steered molecular dynamics, Phys. Chem. Chem. Phys. 13 (2011) 6176–6183.
[41] L.Y. Chen, Glycerol modulates water permeation through *Escherichia coli* aquaglyceroporin GlpF, Biochim. Biophys. Acta Biomembr. 1828 (2013) 1786–1793.
[42] L.Y. Chen, Nonequilibrium fluctuation–dissipation theorem of Brownian dynamics, J. Chem. Phys. 129 (2008).
[43] D.F. Savage, P.F. Egea, Y. Robles-Colmenares, J.D.O.C. Iii, R.M. Stroud, Architecture and selectivity in aquaporins: 2.5 Å X-ray structure of aquaporin Z, PLoS Biol. 1 (2003) e72.